

Theory of the transmission properties of an optical far-field superlens for imaging beyond the diffraction limit

Stéphane Durant, Zhaowei Liu, Jennifer M. Steele,* and Xiang Zhang

5130 Etcheverry Hall, National Science Foundation Nano-scale Science and Engineering Center University of California, Berkeley, California 94720-1740

Received July 22, 2005; revised November 7, 2005; accepted November 21, 2005; posted December 2, 2005 (Doc. ID 63657)

A conventional optical superlens for imaging beyond the diffraction limit produces images only in the near-field zone of the superlens. In contrast, an optical far-field superlens (FSL) device has a remarkable transmission property that leads to a one-to-one relationship between the far-field and the near-field angular spectra. This property makes the device suitable for imaging beyond the diffraction limit from far-field measurement. This specific FSL is composed of a properly designed periodically corrugated metallic slab-based superlens. Through the numerical design and parameter study, we show that the transmission property of this FSL is based on a specific strong-broadband wavenumber excitation of surface-plasmon polaritons supported by the nanostructured metallic grating. © 2006 Optical Society of America

OCIS codes: 110.0180, 160.3900, 230.1950, 310.6860.

1. INTRODUCTION

In a conventional optical imaging system using lenses, transverse resolution is fundamentally limited by the diffraction limit, which is typically about half the wavelength of the light with a normal incidence exposure. This fundamental limit occurs when only propagating waves radiated by an object are collected, which is the case with a conventional imaging system using lenses. The key point in imaging with resolution below the diffraction limit lies on the collection and detection of both propagating and evanescent waves radiated by the object in the near field.¹ A monochromatic plane wave U in free space with a refractive index n can be written as $U = U_0 \exp[i(kx + \gamma z - n2\pi ct/\lambda_0)]$ inside a two-dimensional system (for the sake of simplicity) where λ_0 and c are the wavelength and speed of the light in vacuum, respectively; and k and γ are the transverse and longitudinal wavenumbers, respectively, that form the wave vector $\mathbf{k} = (k, \gamma)$ in the (x, z) Cartesian axis. For a plane wave satisfying Maxwell's equations, transverse and longitudinal wavenumbers must satisfy $k^2 + \gamma^2 = n^2 k_0^2$, with $k_0 = 2\pi/\lambda_0$. Propagating plane waves are characterized by transverse wavenumbers such that $|k| \leq nk_0$, letting γ be a purely real number; on the other hand, evanescent waves are characterized by $|k| > nk_0$, which sets γ as a purely imaginary number, leading to a decay of the amplitude along the z axis. By having larger spatial frequencies than propagating waves, evanescent waves carry the fine details of the object with a resolution below the diffraction limit.

A few years ago² it was predicted that a simple planar thin film termed a *superlens* can be used to produce optical images with resolution below the diffraction limit. Optical imaging with resolution below the diffraction limit

using a silver superlens was recently experimentally demonstrated.^{3,4} For instance in Ref. 3, a 120 nm periodic grating object and a lines object were successfully imaged 75 nm away from the object. The key in superlens imaging is the remarkable ability of a planar superlens to substantially transport a large bandwidth of evanescent waves in transmission from the bottom side to the top side of the slab. This is in contrast with a conventional lens imaging for which evanescent waves decay before reaching the image plane. The excitation of surface-plasmon polaritons (SPP) at both interfaces of an optical superlens made of a noble metal play a key role in the enhancement of evanescent waves.

Although the use of a superlens is very promising for numerous possible applications, such as ultrahigh-density optical lithography, subwavelength sensing, nanofabrication, and related areas, imaging using the current superlens is limited in the near-field zone, as demonstrated in Ref. 5 in the case of a negative-index metamaterial. In a recent letter and proceedings,^{6,7} we proposed a theoretical way to overcome this limitation using a new device termed a far-field superlens (FSL), which is a properly designed periodically corrugated superlens. In this paper, we recall the remarkable transmission properties of the FSL and compare it to a conventional superlens. By using a FSL positioned in the near field of an object and by measuring the angular spectrum scattered in the far field (for instance, using diffraction microscopy⁸), an image of the object can be reconstructed with ultrahigh resolution below the diffraction limit.

It should be noted that another approach has been demonstrated that is capable of imaging with resolution below the diffraction limit using a metallic film⁹ or a photonic-crystal material.¹⁰ In these approaches, surface

waves generated by an object under illumination above the interface of the film can be imaged and magnified with an in-plane lens. In contrast, a FSL projects an image in the far-field, out-of-object plane.

For the self-consistency of this paper, we briefly report the FSL imaging principles in Section 2. The design and the main transmission characteristics of an optical FSL made of silver–glass are developed in Section 3. In Section 4 we present the numerical field-image reconstruction of objects with various near-field distributions from far-field data transmitted by the FSL. The physical mechanisms leading to the unique near-field–far-field angular-spectrum conversion of this FSL optical device are based on a strong excitation of leaky modes of surface-plasmon polaritons with a selective and broadband excitation of wavenumbers. Subsequently, the effects of SPP are computed directly from the field-transmission factor through the metal nanostructure. This parameter study, presented in Section 5, gives substantial physical insight and helps to understand how to design a FSL.

2. FAR-FIELD SUPERLENS IMAGING THEORY

Imaging below the diffraction limit using a planar superlens is limited in the near-field zone of the superlens.⁵ This limitation is simple to understand; evanescent waves are enhanced in transmission, as shown in Fig. 1(a), but remain localized in the near field, meaning that their amplitudes decay exponentially in the normal direction of the superlens, which makes subwavelength imaging in the far field impossible.

In contrast, a FSL not only substantially enhances evanescent waves but also converts them in transmission into propagating waves as shown in Fig. 1(b). A FSL is based on a properly designed periodically corrugated su-

perlens. Waves radiated by an object are transmitted through the grating in several orders of diffraction, following the grating law $k' = k + \Lambda p$, where k' and k are the transmitted and incident transverse wavenumbers, respectively; $\Lambda = 2\pi/d$ is the grating wavenumber, where d is the periodicity; and p is the diffraction order. We are interested only in waves transmitted in the far field, i.e., far enough from the FSL and the object plan that the contribution of evanescent waves vanishes completely. Consequently, only transmitted waves with $|k'| < nk_0$ should be considered, where n is the refractive index of a nonabsorbing free space in which the far-field measurement takes place. A subwavelength period is chosen such that incident propagating waves are transmitted into the far field only through the order 0 and incident evanescent waves with positive (negative) transverse wavenumbers are transmitted in the far field only through the order -1 (order $+1$). The structure is designed such that incident evanescent waves are enhanced by taking advantage of the superlens effect and are also converted into propagating waves using a highly efficient diffraction process into the order -1 . Comparatively, incident propagating waves are transmitted through the order 0 with smaller amplitude. As a result, whereas the near-field angular spectrum radiated by an object contains both propagating and evanescent waves, the main contribution of waves transmitted into the far field through the superlens grating comes from the incident evanescent waves. There is also a one-to-one relationship between sets of transmitted and incident transverse wavenumbers. For instance, by measuring the amplitude of a plane wave transmitted in the far field in a specific direction with a transverse wave number k' , one can deduce unambiguously that the original transverse wave number radiated by the object is $k = k' + \Lambda$. Also, the near-field angular spectrum can be retrieved from the far-field angular spectrum if the -1 order transmission transfer function of the FSL is known.

This one-to-one relationship means that the waves scattered in the far field provide a unique image of the evanescent component of the near field of the object. However, this far-field image is not a direct real-space image of the near field. But one can imagine an experimental setup that would form a real-space image, taking advantage of the Fourier transform properties of classical lens and additional diffractive optics. Without this experimental scheme, one can still compute a real-space image of the local field distribution above the object using an inverse Fourier transform if both phase and amplitude can be measured. However, the measurement of both amplitude and phase of the optical signal is a practical difficulty. This problem also occurs in the optical diffraction microscopy⁸ (or tomography) where the far-field angular spectrum must be measured. In Ref. 8 an experimental setup is proposed in which the angular spectrum is measured by positioning a CCD camera in the Fourier plane of a lens, while a reference beam with an oscillating phase overlaps and interferes with the image. Both phase and amplitude of the angular spectrum can be measured this way, so that a real-space image can be deduced from a simple Fourier transform. This would form the basis of a powerful imaging method with a resolution well below the diffraction limit.

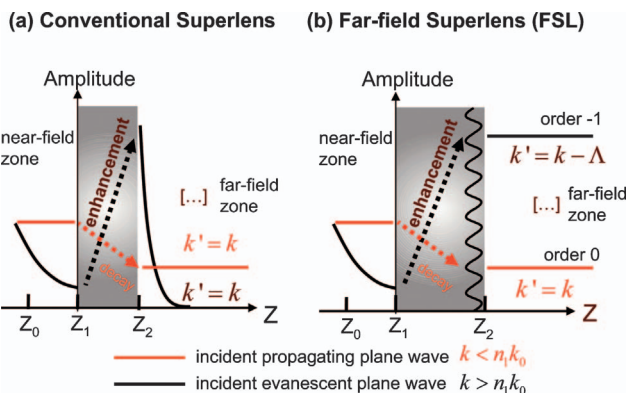


Fig. 1. Transmitted properties of (a) a conventional superlens versus (b) a FSL. It is assumed that waves are radiated by an object at $z = z_0$. Incident evanescent waves are enhanced in transmission through a conventional superlens (a) and still vanish quickly in the near-field zone, limiting the imaging ability of a superlens to the near field. In contrast, a FSL (b) both enhances and converts the original evanescent waves in propagating waves. In this latter case, incident propagating waves are comparatively transmitted with low amplitude in the far field, and the main contribution to the far-field angular spectrum is due to the incident evanescent waves. Using this property, the near-field angular spectrum can be retrieved from the measurement of the far-field angular spectrum.

3. DESIGN OF AN OPTICAL FAR-FIELD SUPERLENS DEVICE

A. Transmission Properties

In this section we describe the design and transmission behavior of an optical FSL made of silver–glass that satisfies all criteria mentioned in Section 2. The operating wavelength is 376 nm, and the period $d=150$ nm sets the grating wavenumber to be $\Lambda \approx 2.5k_0$. A rectangular silver grating of 55 nm height with a metal-filing ratio $f = 0.3$ is supported by a 35 nm thickness silver slab, as shown in Fig. 2. The choices of the wavelength and the geometric parameter of this silver grating are detailed in Section 5. We assume that a cylindrical object positioned below the superlens in the near-field zone inside the glass is exposed by a p -polarized light, such that we consider a planar scattering with a wavenumber $\mathbf{k}=(k, \gamma)$ in the (x, z) Cartesian axis and the H field is oriented along the y axis. The field scattered above the object is described by an angular spectrum of magnetic field noted $\tilde{H}_1(k, z)$, where the tilde is a notation for the Fourier transform along the x axis. The angular spectrum transmitted above the FSL noted $\tilde{H}_2(k', z_2)$ is the result of the superposition of incident waves $\tilde{H}_1(k, z)$ transmitted through all diffraction orders of the grating

$$\tilde{H}_2(k', z_2) = \sum_{p=-\infty}^{+\infty} t_p(k_p) \tilde{H}_1(k_p, z_1), \quad \text{where } k_p = k' - p\Lambda. \quad (1)$$

In Eq. (1), $t_p(k)$ is the p -order field transfer function of the FSL. Transfer functions were computed by solving numerically Maxwell's equations from the rigorous coupled-wave analysis (RCWA)^{11,12} using experimental permittivity data of glass $\epsilon_g=2.31$ and silver¹³ $\epsilon_{Ag}=-3.16-0.2i$. In this method, in each layer, the permittivity and the electric and magnetic fields are expanded in series of N space-harmonic grating modes where the p th order transverse wavenumber is given by $k_p=k+p\Lambda$, with p from $-(N-1)/2$ to $+(N-1)/2$, and k is the incident transverse wave-

number. The boundary conditions at the interface of each layer compose a system of independent equations leading to a unique solution. This system can be solved using algorithms provided in Refs. 11 and 12, and a good convergence can be obtained with a low N number of modes when a subwavelength grating is considered. The accuracy of the numerical solution obtained with $N=51$ has been tested using the theorem of reciprocity of electromagnetic waves^{14,15} and was applied for both propagating and evanescent waves. Figure 2 shows the transfer function for p polarization for order 0 (black curve), -1 (red curve), and -2 (blue curve). It is clear that $|t_0(k)| \ll |t_{-1}(k+\Lambda)|$ and $|t_{-2}(k+2\Lambda)| \ll |t_{-1}(k+\Lambda)|$ for positive transverse wavenumbers of propagating plane waves, which satisfy the requirement $0 < k < nk_0$. Larger-order transfer functions are not shown, because their amplitudes are negligible. Because the grating is symmetrical, we have $t_p(k) = t_{-p}(-k)$. Consequently, we also have $|t_0(k)| \ll |t_{+1}(k-\Lambda)|$ and $|t_{+2}(k-2\Lambda)| \ll |t_{+1}(k-\Lambda)|$, with negative transverse wavenumbers satisfying $-nk_0 < k < 0$. As a result, only one order is kept in the summation of Eq. (1), so this equation is reduced to

$$\tilde{H}_2(k', z_2) = \begin{cases} t_{-1}(k'+\Lambda) \tilde{H}_1(k'+\Lambda, z_1) & \text{with } 0 < k' < nk_0 \\ t_{+1}(k'-\Lambda) \tilde{H}_1(k'-\Lambda, z_1) & \text{with } -nk_0 < k' < 0 \end{cases}. \quad (2)$$

Equation (2) shows that there is a one-to-one relationship between the near-field angular spectrum below the FSL and the far-field angular spectrum above the FSL. The near-field angular spectrum $\tilde{H}_1(k, z < z_1)$ can be retrieved, using Eq. (2), from the measurement of both phase and amplitude of the far-field angular spectrum $\tilde{H}_2(k', z > z_2)$ and knowing both amplitude and phase of the -1 order transfer functions (Fig. 2).

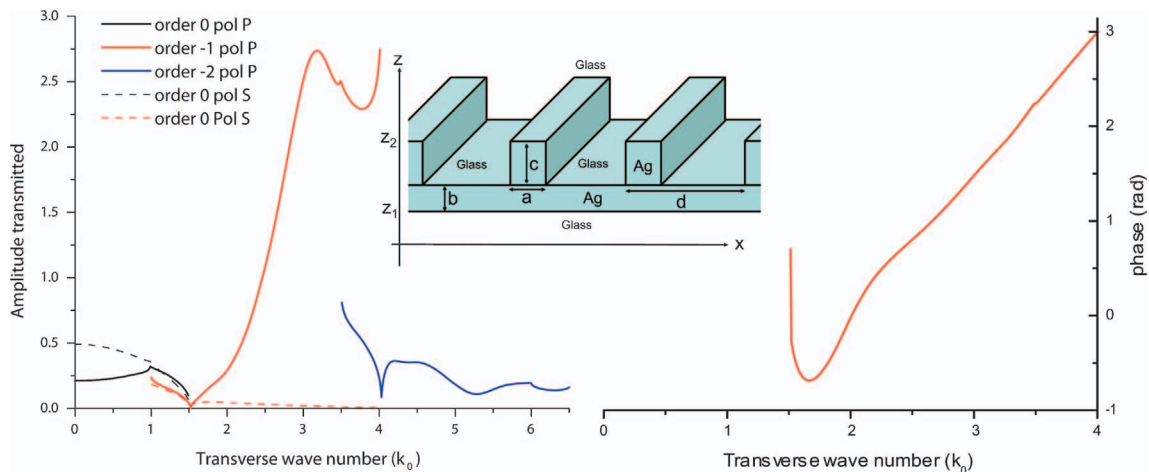


Fig. 2. Final design of a silver FSL working at $\lambda_0=376$ nm, with the following parameters: $a = 45$ nm, $b = 35$ nm, $c = 55$ nm, and $d = 150$ nm. Left, the amplitude of the transmission factor through orders $p = 0$ (black), $p = -1$ (red), and order $p = -2$ (blue) from planes $z = z_1$ to $z = z_2$ for s (dashed curves) and p (solid curve) polarizations. It can be seen that evanescent waves are transmitted in the far field with large amplitudes through the order -1 , whereas the transmission of incident propagating waves are blocked through the order 0. Right, the phase delay of the transmission through the order -1 , revealing a linear dependence with k .

B. Bandwidth of Measurement

The shift of transverse wavenumber for the conversion of evanescent into propagating waves is set by the grating wavenumber, $\Lambda \approx 2.5k_0$ in this example, where the wavelength is 376 nm and the periodicity is $d = 150$ nm. This is fundamental for the image-reconstruction processing using Eq. (2) and sets the bandwidth of measurement of the angular spectrum. If the far-field angular spectrum can be measured for k with a maximum value of $k = 1.5k_0$, assuming an optical system with a numerical aperture NA = 1.5 (i.e., embedded in a medium with a refractive index $n = 1.5$), the largest k that can be retrieved is $k' = k + \Lambda = (1.5 + 2.5)k_0 = 4k_0$. By using this specific silver FSL, the bandwidth of the near-field angular spectrum that can be measured is $\Delta k = 8k_0$. Consequently, a far-field optical imaging could be achieved with an expected resolution $\Delta x \approx \lambda_0/8$, on the image of the electromagnetic energy distribution using $\Delta k \Delta x \approx 2\pi$, which is well beyond the diffraction limit. For comparison, the best resolution that could be obtained on the image of the electromagnetic energy distribution with a diffraction-limited classical microscope is $\Delta x \approx \lambda_0/3$, with a numerical aperture NA = 1.5.

Because this optical FSL is a symmetric grating, we know that . So by looking at the shape of $|t_{-1}(k)|$ for positive k , we can deduce that $|t_{-1}(k' + \Lambda)| \approx |t_{+1}(k' - \Lambda)|$ for small $k' \in [-0.2; 0.2]k_0$ corresponding to waves scattered in the direction close to the normal incidence. Inside this small bandwidth $k' \in [-0.2; 0.2]k_0$, there is an overlap of waves scattered in the same direction, and this data cannot be used to retrieve unambiguously the field above the object below the FSL. In contrast, with $k' > 0.2k_0$ and $\Lambda = 2.5k_0$, we have $|t_{-1}(k' + 2.5k_0)| \gg |t_{+1}(k' - 2.5k_0)|$. Therefore the overlap of waves is negligible when $k' > 0.2k_0$, with the respective incident wavenumbers $k' + 2.5k_0$ and $k' - 2.5k_0$ transmitted in the far field in the same direction k' through orders -1 and $+1$.

Assuming that the field transmitted in the far field $\tilde{H}_2(k', z)$ can be measured in the bandwidth $k' \in [-1.5; -0.2] \cup [0.2; 1.5]k_0$, the near-field angular spectrum above the object $\tilde{H}_1(k, z)$ can be retrieved in the bandwidth $k \in [-4; -2.7] \cup [-1.5; +1.5] \cup [2.7; 4]k_0$, where the center part $[-1.5; +1.5]k_0$ is assumed to be measured without the FSL. The field in real space $H_1(x, z)$ can then be computed using an inverse Fourier transform, leading to a resolution $\Delta x \approx \lambda_0/8$ using this specific FSL.

4. IMAGING RECONSTRUCTION BEYOND THE DIFFRACTION LIMIT

This section deals with the real-space imaging reconstruction of the object. We show that the measurement of far-field angular spectrum using a FSL can be used to reconstruct a near-field image of the local field distribution, with a resolution below the diffraction limit. In practice, the far-field angular spectrum can be measured at any large distance (compared with the wavelength) from the object. It could be measured by imaging the object and the FSL in the Fourier plan of a classical lens, following, for instance, the setup proposed in Ref. 8. We first simulate exactly the forward problem, that is, the computation of the scattering by an object by itself and when the optical

FSL is positioned above the object in order to generate the far-field data that could be measured experimentally. Then the image retrieval is computed from the direct analytic inversion of Eq. (2).

A. Forward Computation: Near-Field to Far-Field Angular Spectra above the Object with and without a FSL

Let us consider the case of an object composed by a 40 nm two-line source of coherent 376 nm wavelength TM waves separated by a 50 nm gap. A unity value of the H magnetic field is assumed on the two-line source and vanished everywhere else. The optical FSL designed previously (see Fig. 2) is assumed to be positioned 20 nm above the object. First, the angular spectrum of the near field scattered by the two-line source noted $\tilde{H}_1(k, z)$ is computed 20 nm above the object (right below the silver film interface) using the rigorous diffraction theory,¹⁶ and the result is reported in Fig. 3(a). Whereas the evanescent components $|k| > 1.5k_0$ of the spectrum vanished quickly at larger distances, the propagating components $|k| > 1.5k_0$ are unchanged along the propagation, so the amplitude far-field angular spectrum is exactly the same as the one in near-field, with $|k| < 1.5k_0$. The transmitted far-field angular spectrum $\tilde{H}_2(k', z)$ scattered by the FSL is computed rigorously by using Eq. (1) and the exact result of the field transfer functions $t_p(k)$. The result, reported in Fig. 3(b), is compared with the scattered angular spectrum in the far field without the FSL. These two results provide a complete set of data that simulates a measured signal in an experiment and are subsequently used as the known data for the near-field image reconstruction.

B. Near-Field Imaging Reconstruction from the Far-Field Angular Spectrum

The designed silver FSL processes a unique one-to-one $k' \rightarrow k$ relation, as shown by Eq. (2). This unique simplicity allows us to use the forward data described in Subsection 4.A in order to retrieve the near-field angular spectrum unambiguously at $z = z_1$ just below the FSL. As mentioned before in Subsection 3.B, the near-field angular spectrum $\tilde{H}_1(k, z_1)$ can be retrieved with $k \in [-4, -2.7] \cup [2.7, 4]k_0$ using Eq. (2) from the measurement of the far-field angular spectrum data $\tilde{H}_2(k')$ with $k' \in [-1.5, -0.2] \cup [0.2, 1.5]k_0$. The central band $[-0.2, +0.2]k_0$ has been omitted because of an overlap of waves transmitted in the same direction through orders -1 and $+1$, as mentioned previously. The near-field angular spectrum is shown in Fig. 3(c). The propagating components with $k \in [-1.5, 1.5]k_0$ of $\tilde{H}_1(k, z_1)$ were used to complete the central band of the angular spectrum from the far-field data previously computed without FSL. The real-space field distribution above the object and below the FSL $z_0 < z < z_1$ is then obtained by using the rigorous diffraction theory and applying an inverse Fourier transform. This result is reported in Fig. 3(d) as the distribution of the density of electromagnetic energy 5 nm above the object.

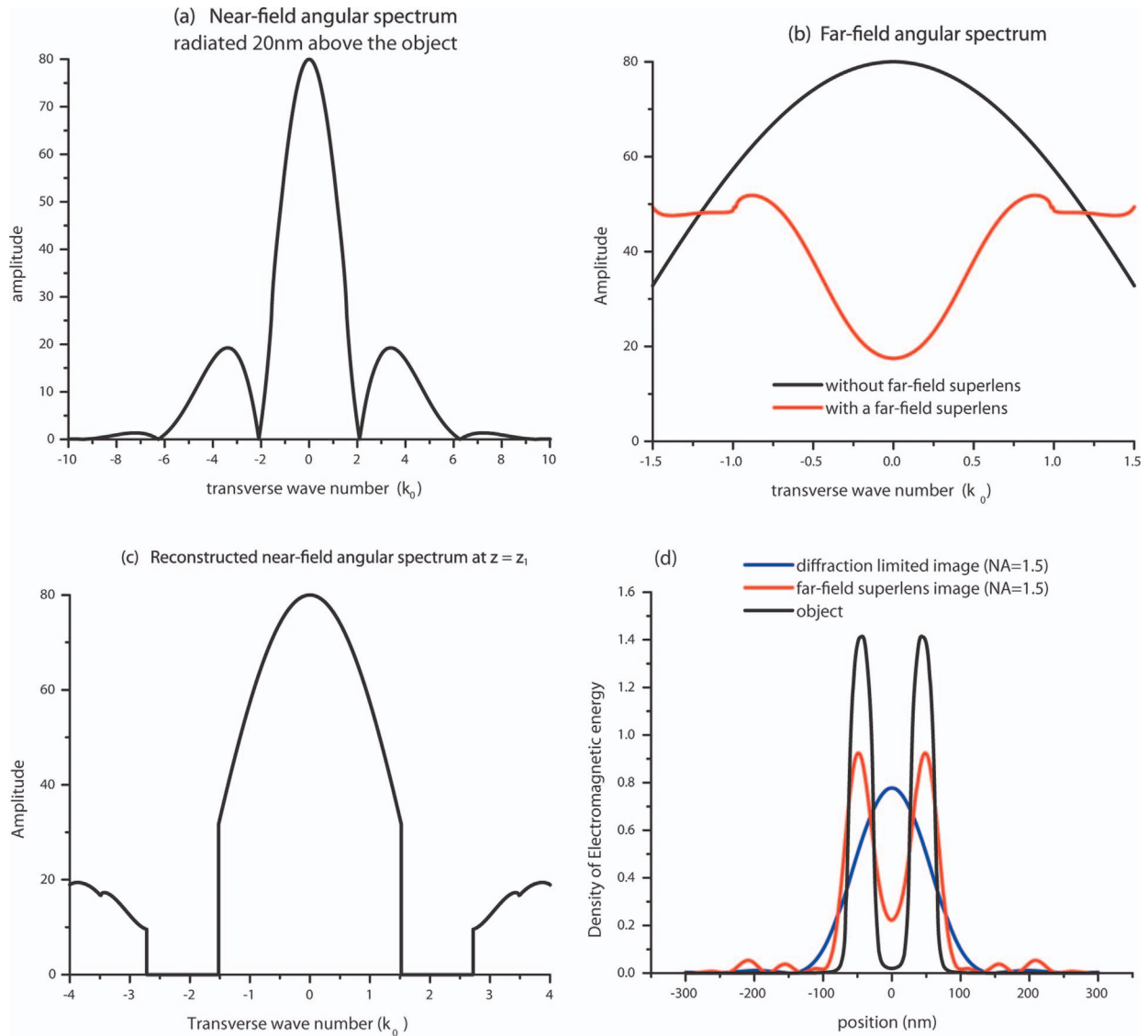


Fig. 3. Two lines of a source object of 40 nm width and 50 nm gap are used for (a), (b) the exact computation of the far-field angular spectrum and (c) the retrieval of the near-field angular spectrum image and (d) the real space image using a FSL from the far-field data assuming $NA = 1.5$.

This result can be compared with the exact distribution radiated by the two-line source object (in black) obtained using the rigorous diffraction theory, showing that the FSL provides a faithful image. We also computed the result of the diffraction-limited image using values of $\tilde{H}_1(k, z_1)$ with k inside the propagating bandwidth $[-1.5, 1.5]k_0$. The comparison with the diffraction-limited image clearly shows that the image resolution obtained using a FSL is far beyond the diffraction limit. Following exactly the same procedure, we have also computed the image reconstruction of a nonsymmetrical object composed by a set of 50 nm line source separated by a 30–80nm gap, as shown in Fig. 4. Note that the values of the reconstructed local density of energy shown in Figs. 3 and 4 are normalized such that the total densities of energy integrated along the x axis are the same as the object.

The image reconstructed using the FSL is in good agreement with the object source distribution. However, because the band $[1.5, 2.7]k_0$ is missing for the recon-

struction of the near-field angular spectrum, some artefacts might appear for spatial details between 70–125 nm in the real-space image. If the field distribution scattered by an object contains nonnegligible angular spectrum within the bandwidth $[1.5, 2.7]k_0$, then the field distribution will not be properly retrieved in real space. This incorrect reconstruction can happen mainly for periodic or quasi-periodic objects for which the angular spectrum is discrete and could be fully contained within the missing band. For other field distributions like the two-line source, the angular spectrum is broad enough that a large part of the spectrum can be retrieved, except the missing band. The second and third peaks in Fig. 4 of the reconstructed image are slightly larger than other peaks because of the missing band, leading to an imperfect reconstruction. Also, because of this missing band, the reconstruction of the two-line source separated by a 120 nm gap is much more difficult, as shown in Fig. 4. Nevertheless, even in this difficult case, the FSL provides a bet-

ter image compared with a diffraction-limited classical microscope.

5. ROLE OF SURFACE-PLASMON POLARITONS ON THE TRANSMISSION OF PROPAGATING AND EVANESCENT WAVES BY A METAL-DIELECTRIC FAR-FIELD SUPERLENS

Until this point in this paper, we have discussed only the transmission properties of a superlens and a FSL in terms of input–output, without explaining the intrinsic physics hidden behind these remarkable behaviors. The superlens theory predicted that a slab of negative-index material can significantly enhance evanescent waves in transmission. A full recovery of the Fourier components, including evanescent waves, can be used for imaging with resolution well below the diffraction limit. This enhancement can be achieved by excitation of surface-wave resonances, depending on the materials and geometry used. A superlens can be constructed from metamaterial with effective negative-index media,^{17,18} and (dielectric^{19–21} or metallic²²) photonic crystals as well as a slab of natural material^{2–4,23} that supports a surface-wave polariton. The superlens effect has been reported experimentally for microwave regime²⁴ using a two-dimensional photonic crystal. Recently, optical superlens imaging has been demonstrated³ experimentally using a silver slab.

In this section, we will discuss the specific case of a FSL composed of metal and dielectric media. The design of a FSL is satisfying, since the transmission and conversion of incident evanescent waves into propagating waves through a unique negative order of diffraction is very large, compared with the transmission of incident propagating waves through the order 0. The design of one particular FSL, as shown in Fig. 2, satisfies the latter requirement, which can be written mathematically as $|t^0(k)| \ll |t^{-1}(k+\Lambda)|$, with $0 < k < nk_0$, as mentioned before. The FSL is constituted by a silver–glass grating of 55 nm height, 150 nm periodicity, and a metal filling ratio 0.3, supported by a 35 nm thickness silver slab. The entire

sample is covered in both sides by glass. We would like to answer to the question why such a structure transmits light strongly in the order -1 for incident evanescent waves, whereas the transmission of propagating wave in order 0 is comparatively very small. The role of SPP is considered first in the case of a planar metal film and subsequently for the case of a metal film periodically corrugated.

A. Transmission by a Planar Metal Superlens (*p*-Polarization)

At a metal–dielectric interface, SPPs are the coupling of *p*-polarized surface electromagnetic waves with $k > nk_0$ (propagating along the interface) and the induced collective excitation of free electrons at the boundary. The essential role of SPPs in the enhancement of evanescent waves in transmission by a planar film made of a noble metal with $\text{Re}(\epsilon) < 0$ like silver at optical wavelength has been clearly established both theoretically and experimentally.^{25–28} A metal film can enhance evanescent waves in transmission by a resonant *p*-polarization excitation of SPP at both interfaces, which can couple depending on the thickness of the slab. We report the *H*-field transmission factor in Fig. 5 as function of the optical wavelength and the transverse incident wavenumber through a silver film about 35 nm that separates two half-spaces of glass. The maximum positions of the transmission factor reveal the excitation of the SPP modes. Two modes can be distinguished, which we term k_{sp}^+ and k_{sp}^- where $k_{sp}^+(\lambda_0) > k_{sp}^-(\lambda_0)$. It is known that the gap $k_{sp}^+(\lambda_0) - k_{sp}^-(\lambda_0)$ increases for smaller thickness, and that SPP with larger k can be excited in transmission for smaller thickness. The thickness of the film is a very important criterion if one wants to design a superlens with a broadband-large enhancement in transmission of evanescent waves. With a silver slab of 35 nm covered by glass, it can be seen in Fig. 5 that a relatively flat transmission as a function of k can be obtained at a wavelength close to 365 nm and below 390 nm. This broadband of k for which there is an enhancement of evanescent waves is a key

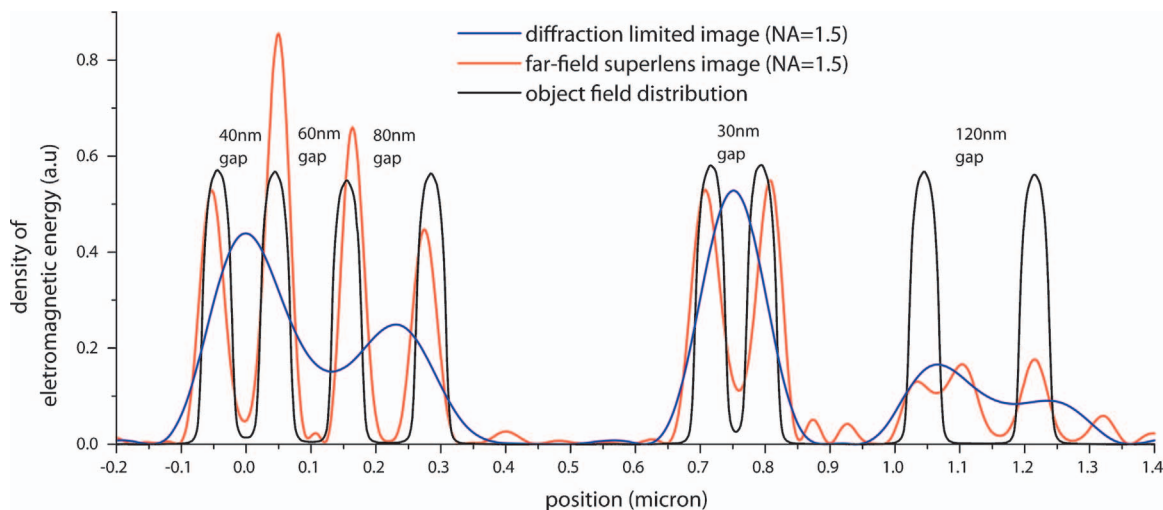


Fig. 4. Density of electromagnetic energy 5 nm above the object and near-field images retrieved from far-field data assuming $NA = 1.5$ with and without FSL. The object is constituted by a set of 50 nm width lines source separated by a 30–120 nm gap. This rigorously computed result directly demonstrates the imaging resolution below the diffraction limit using a FSL with an arbitrarily shaped object.

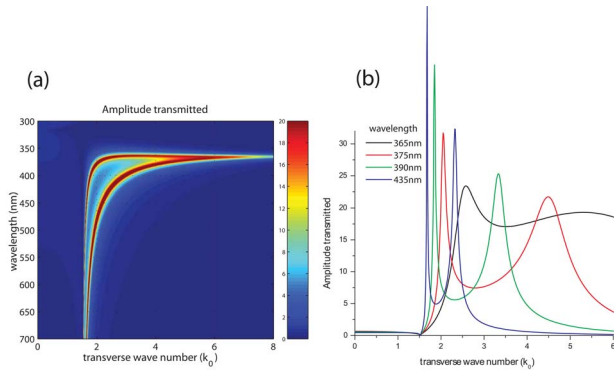


Fig. 5. (Color online) Transmission factor shown through an interface through a silver film of 35 nm thickness in glass as a function of the optical wavelength and the transverse wavenumber. Two sharp modes of SPP are clearly shown for the large wavelength at 435 nm. The bandwidth of modes increases for a wavelength reaching 365 nm, for which resonances are superimposed.

point for imaging purposes with a superlens. This property was largely exploited, as mentioned in Ref. 23, on the near-field imaging experimental demonstration using a silver slab superlens.^{3,4}

B. Negative Role of SPP on the Far-Field 0-Order Transmission of a FSL

The comparison of the amplitude transmitted through order 0 of *s* and *p* polarizations, plotted in Fig. 2 for propagating waves close to normal incidence $k = k' \approx 0$, shows that the amplitude transmission factor through the FSL is twice as large with *s* compared to *p* polarization. Consequently, the flux transmitted is 4 times larger with *s* polarization. To explain this phenomenon, we can model the transmission in the forward direction in the order 0, considering that the amplitude transmitted is due mainly to the direct transmission of waves (without a multiple-scattering process), and the sums of waves doubly scattered first in the order +1 of the grating and then scattered back in the original direction using the order -1. Larger multiple-scattering processes can be negligible. Incident *p*-polarized waves that are multiply scattered can excite several modes of SPP. The excitation of these SPP modes leads to a field enhancement of surface waves but also leads to a large increase of the absorption factor. Because SPPs cannot be excited with an *s*-polarized field, no field enhancement due to SPPs can be invoked with *s* polarization. From additional calculation (not shown in this paper) of the total absorption through the FSL, we found out that the absorption factor is 5 times larger for *p* compared with *s* polarization. This effect was also observed experimentally in the study of the enhanced light transmission through two-dimensional periodic arrays of subwavelength holes in a metal film.²⁹ In this experiment, the large transmission factor due to the excitation of SPPs was systematically followed by a large absorption factor. Nevertheless, with the optical device studied in this paper, the transmission factor through order 0 is not enhanced with *p* compared with *s* polarization. But as it has been described in a theoretical work,³⁰ the excitation of SPPs in *p* polarization can lead to a negative role in 0 order transmission by metallic gratings with subwave-

length slits. We believe that the normal incidence transmission through the FSL is reduced with *p* compared with *s* polarization, because of a larger absorption and a negative role of SPP in the transmission factor.

C. Role of SPP on the Large-1-Order Transmission with *p*-Polarized Waves of FSL

Transfer functions of order -1 for both *s* (dashed curves) and *p* (solid curves) polarizations are plotted in Fig. 2. For incident evanescent waves with $k > 2k_0$, while the transmitted amplitudes of *p*-polarized waves are large, the transmitted-amplitude *s*-polarized waves are almost equal to zero. This result clearly shows the fundamental role of SPP on the large transmission through the diffraction order -1 of the grating.

Let us now look at the amplitude transmitted through the silver FSL for *p* polarization of diffraction order 0 and -1 as a function λ_0 and k , as shown in Fig. 6. It can be seen that a large transmission through the order -1

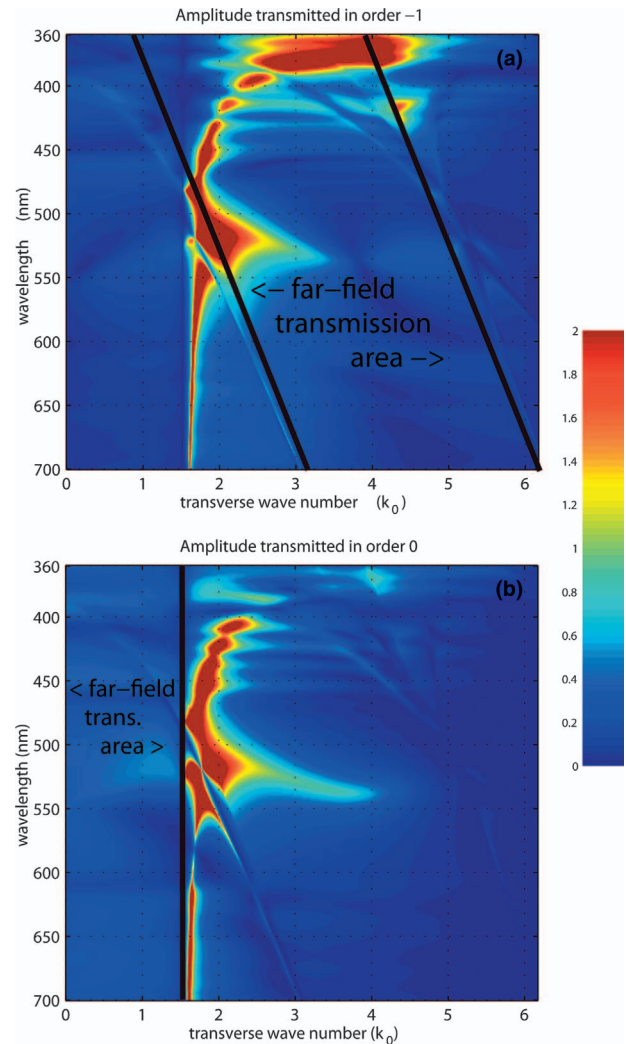


Fig. 6. Transfer function of (a) order 0 and (b) -1 of the silver-glass grating FSL described in the Fig. 2 caption as a function of the wavelength, with $a = 45$ nm, $b = 35$ nm, $c = 55$ nm, and $d = 150$ nm. The black lines show the area for which waves are transmitted in the far field. With these parameters, the FSL is well designed to work with wavelengths between 365 and 390 nm.

within a large bandwidth of $k > 2k_0$ can be obtained for wavelengths from 365 to 390 nm. This result is similar to the case of a simple 35 nm thick silver film, except that interestingly, at these wavelengths through the diffraction order 0 of the FSL, there is no particularly large enhancement of evanescent waves for $k > 2k_0$. Actually, a computation of the field distribution inside the multilayer grating (result not shown in this paper) suggests that incident evanescent waves are transmitted with large amplitude, from the bottom to the top of the 35 nm silver film. These evanescent waves are in part lost 55 nm above the slab along the grating area and are in part diffracted by the grating. Consequently, amplitudes of evanescent waves transmitted through the order 0 are low just above the grating at the plane $z = z_2$ (where the transmission factor was defined).

1. Role of the Metal-Film Thickness on the Field Enhancement

Along the design of the silver FSL at the working wavelength 376 nm, we found that the optimum thickness of the silver slab was 35 nm, keeping other size parameters of the grating unchanged with the grating depth $c = 55$ nm and metal filing ratio $f = 0.3$. The transfer functions of order 0 and -1 are reported in Fig. 7 as a function of the silver slab thickness from 0 to 100 nm. A large transmission in the order -1 is obtained when the silver film is between 30 and 40 nm thickness, demonstrating that the large transmission in order -1 could not be built without the silver slab. There is little doubt that the large transmission is due to the SPP excitation that builds an enhancement of evanescent waves before conversion in propagating waves by scattering in the grating, because of the following arguments: This enhancement does not occur with s -polarized waves, and it is known experimentally³ that 35 nm thick silver film used as a superlens has the properties to enhance evanescent waves with $k > 2.5k_0$ and $\lambda_0 = 365$ nm [see also, for instance, Fig. 5], because of the SPP excitation. However, it is surprising that the optimum thickness of the silver slab in the FSL is the same as that for a conventional silver superlens. This result is surprising because the dispersion relation of SPP on a simple silver slab is theoretically known³¹ to be strongly modified by the presence of roughness, or a grating on top of the slab. It is claimed in Ref. 31 that a small roughness limits the superlens effect, because evanescent waves are no longer as enhanced. Although it is clear that the SPP modes of a silver film are modified by the grating, our result shows that a large bandwidth of evanescent waves can be strongly excited and transmitted through the order -1 of diffraction.

2. Role of the Metal-Filing Ratio and the Height of the Grating

We investigate the transmission properties of the silver FSL as a function of the metal filing ratio of the grating and the height of the grating, with a constant thickness $b = 35$ nm and a constant period $d = 150$ nm. As shown in Fig. 8, a large transmission in order -1 for a large broadband of incident evanescent wave is achieved if the

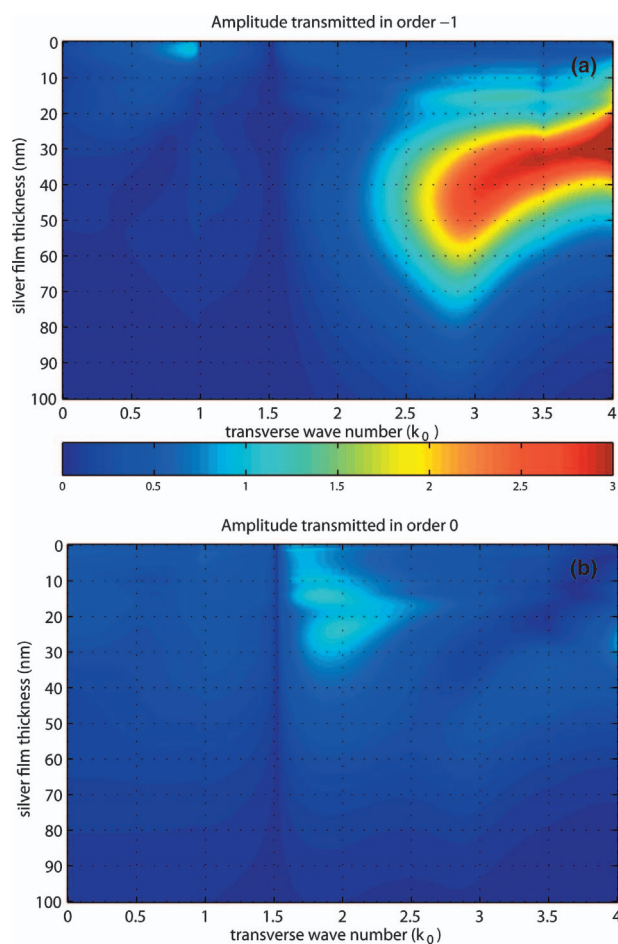


Fig. 7. Transfer function of (a) order 0 and (b) order -1 of the silver–glass FSL at $\lambda_0 = 376$ nm as a function of the thickness of the silver slab with $a = 45$ nm, $c = 55$ nm, and $d = 150$ nm. A maximum of transmission through order -1 is found with 30–40 nm of silver slab. The excitation of SPP modes in the slab of silver at a specific thickness plays a key role in the substantial enhancement of evanescent waves that are converted in propagating waves in the order -1 of the diffraction grating.

filing ratio f is roughly larger than 0.2 and smaller than 0.4 and if the grating depth c is between 30 and 60 nm, with an optimum at 55 nm.

The excitation of SPP modes in the 35 nm thick silver film contributes strongly to build the large amplitude of evanescent waves, but the presence of the grating modifies SPP mode properties into SPP leaky modes, because evanescent waves are diffracted in the far field by the grating. The leaky property of these modes reduces the field enhancement of evanescent waves. The achievement of a large transmission in the order -1 is obtained if an enhancement of evanescent waves is built by the silver slab and if the diffraction process is efficient enough to convert evanescent waves to propagating waves with large amplitude. Intuitively, large diffraction efficiencies would limit the SPP excitation in its role on the evanescent field enhancement, leading to small amplitude transmitted in the order -1 . On the other hand, smaller diffraction efficiencies would improve the role of the SPP on the enhancement of evanescent waves but would decrease the amplitude transmitted in the order -1 . So there should be an optimum diffraction efficiency that leads to

the maximum values of $|t^{-1}(k)|$. The efficiency of the conversion of evanescent waves into a propagating wave can be controlled by the metal filing ratio and the grating depth. Care has to be taken when such a simplified picture is used, because in general SPP modes in the slab are modified by the presence of the grating. A simple way is to consider a grating with a filing ratio small enough so that SPP modes in the 35 nm silver slab would not be drastically modified and a large grating depth to enhance the diffraction efficiency. That is why the small filing ratio $f = 0.3$ and a long grating depth $c = 55$ nm lead to a good compromise for a large-enough field enhancement and a large-enough diffraction efficiency to convert evanescent waves into propagating waves.

D. Spatial-Harmonics Modes Involved in the Far-Field Superlens Effect

The FSL transfer function for order 0 and order -1 were obtained with $N=51$ orders using RCWA. The question that arises is how many modes are necessary to model the remarkable transmission behavior of this optical device. With RCWA, this question can be easily answered by reducing the number of spatial-harmonics modes for which the field is expanded during the computation. As shown in

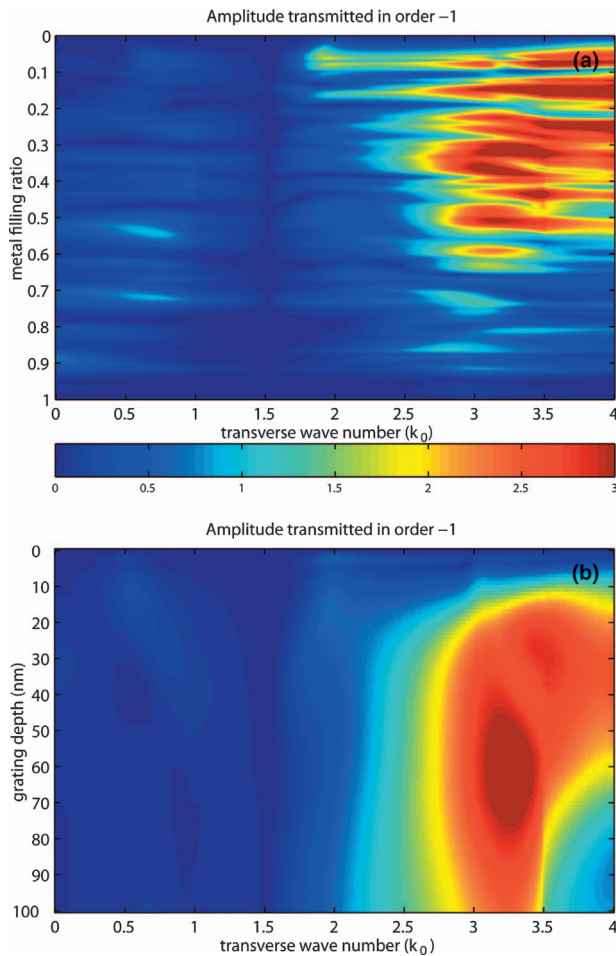


Fig. 8. Amplitude of transmitted waves in diffraction order -1 as a function (a) of the metal filing ratio with $b = 35$ nm, $c = 55$ nm, and $d = 150$ nm and (b) of the grating depth with $a = 45$ nm, $b = 35$ nm, $d = 150$ nm.

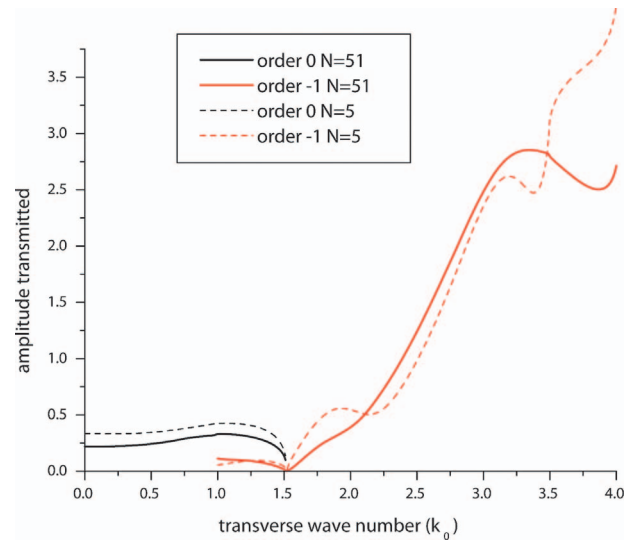


Fig. 9. Computed order 0 and -1 transfer functions of the optical FSL considered, using RCWA with $N=51$ (solid curves) or $N=5$ (dashed curves) spatial-harmonic orders. Interestingly, the enhancement of evanescent waves and conversion into propagating waves through the diffraction order -1 can be built, even considering the low number of spatial-harmonic order.

Fig. 9, using a number of spatial-harmonic modes as low as $N=5$, the strong enhancement and conversion in propagating wave transmission through the diffraction order -1 can be obtained. With $N=5$, only waves with transverse wavenumbers $k_n = k + n\Lambda$ are considered with $n \in [-2, +2]$ (k is the incident transverse wavenumber). This result is important for further modeling of the phenomenon; it shows that only small values of transverse wavenumbers have to be considered involving low orders of multiple-scattering processes.

6. SUMMARY

Since the first theory² and the recent experimental evidence of optical imaging beyond the diffraction limit using a superlens,³ imaging has been fundamentally limited to the near-field zone of the superlens using the conventional scheme. In a previous letter,⁶ a theory was introduced on how to extend the near-field imaging ability beyond the diffraction limit of a superlens to the far field. In this paper we have reviewed the transmission behavior of this new optical device, termed FSL, which has the capability to convert the near-field angular spectrum radiated by an object into a far-field angular spectrum, following a remarkable one-to-one relationship. This unique transmission property allows a unique imaging reconstruction from far-field data using a FSL without scanning the surface. Section 5 of the paper introduced the physics involved in the transmission properties of an optical FSL constituted by metal-dielectric media. To understand how to design a FSL made of metal-dielectric, the basic properties of SPPs in a metallic film were reviewed quickly. In particular, the control of SPP modes by adjusting the thickness of a metallic film is important to design a superlens that can enhance a large bandwidth of evanescent waves. The ability of an optical FSL made of metal-dielectric grating on top of a metal slab to enhance inci-

dent evanescent waves and to convert them efficiently into propagating waves is explained through a parametric study. By using a grating with a small metal filing ratio, the optimal thickness for the silver slab of the FSL was found to be similar to the optimal thickness of a conventional planar superlens. By choosing a grating with a small filing ratio, although the SPP modes supported by a pure silver film are modified by the presence of the grating, the numerical results have shown that a strong enhancement of evanescent waves still occurs in the slab, whereas the grating plays the role of an efficient converter of evanescent waves into propagating waves.

ACKNOWLEDGMENTS

The authors thank Yi Xiong, Yuri Pikus, and Nicholas Fang for helpful stimulating discussions. The authors acknowledge support from the Office of Naval Research by the Multidisciplinary University Research Initiative (ONR grant N00014-01-1-0803) and from the National Science Foundation for the Center for Nanoscale Science and Engineering (grant DMI-0327077).

*Now with the Department of Physics and Astronomy, Trinity University, One Trinity Place, San Antonio, Texas, 78212. S. Durant and X. Zhang are the corresponding authors and can be reached via e-mail at durant@berkeley.edu and xiang@berkeley.edu, respectively.

REFERENCES

- J.-J. Greffet and R. Carminati, "Image formation in near-field optics," *Prog. Surf. Sci.* **56**, 133–237 (1997).
- J. B. Pendry, "Negative refraction makes a perfect lens," *Phys. Rev. Lett.* **85**, 3966–3969 (2000).
- N. Fang, H. Lee, C. Sun, and X. Zhang, "Sub-diffraction-limited optical imaging with silver superlens," *Science* **308**, 534–537 (2005).
- D. O. S. Melville and R. J. Blaikie, "Super-resolution imaging through a planar silver layer," *Opt. Express* **13**, 2127–2134 (2005).
- V. A. Podolskiy and E. E. Narimanov, "Near-sighted superlens," *Opt. Lett.* **30**, 75–77 (2005).
- S. Durant, Z. Liu, N. Fang, and X. Zhang, "Far-field superlens theory for optical imaging beyond the diffraction limit," www.arxiv.org, physics/0601163 (2006).
- S. Durant, Z. Liu, N. Fang, and X. Zhang, "Theory of optical imaging beyond the diffraction limit with a far-field superlens," in *Plasmonics: Metallic Nanostructures and Their Optical Properties IV*, M. I. Stockman, ed. Proc. SPIE **6323**, 63231H (2006).
- V. Lauer, "New approach to optical diffraction tomography yielding a vector equation of diffraction tomography and a novel tomographic microscope," *J. Microsc.* **205**, 165–176 (2002).
- I. I. Smolyaninov, J. Elliot, A. V. Zayats, and C. C. Davis, "Far-field optical microscopy with a nanometer-scale resolution based on the in-plane image magnification by surface plasmon polaritons," *Phys. Rev. Lett.* **94**, 057401 (2005).
- I. I. Smolyaninov, C. C. Davis, J. Elliott, G. A. Wurtz, and A. V. Zayats, "Super-resolution optical microscopy based on photonic crystal materials," *Phys. Rev. B* **72**, 085442 (2005).
- M. G. Moharam, E. B. Grann, D. A. Pommet, and T. K. Gaylord, "Formulation for stable and efficient implementation of the rigorous coupled-wave analysis of binary gratings," *J. Opt. Soc. Am. A* **12**, 1068–1076 (1995).
- M. G. Moharam, D. A. Pommet, E. B. Grann, and T. K. Gaylord, "Stable implementation of the rigorous coupled-wave analysis for surface relief gratings-enhanced transmittance matrix approach," *J. Opt. Soc. Am. A* **12**, 1077–1086 (1995).
- P. B. Johnson and R. W. Christy, "Optical-constants of noble-metals," *Phys. Rev. B* **6**, 4370–4379 (1972).
- R. Carminati, M. Neito-Vesperinas, and J.-J. Greffet, "Reciprocity of evanescent electromagnetic waves," *J. Opt. Soc. Am. A* **15**, 706–712 (1998).
- R. Carminati, J. J. Saenz, J.-J. Greffet, and M. Nieto-Vesperinas, "Reciprocity, unitarity, and time-reversal symmetry of the *S* matrix of fields containing evanescent components," *Phys. Rev. A* **62**, 012712 (2000).
- J. W. Goodman, *Introduction to Fourier Optics*, 2nd ed. (McGraw-Hill, 1996), Chap. 3.
- R. A. Shelby, D. R. Smith, and S. Schultz, "Experimental verification of a negative index refraction," *Science* **292**, 77–79 (2001).
- V. M. Shalaev, W. Cai, U. Chettiar, H.-K. Yuan, A. K. Sarychev, V. P. Drachev, and A. V. Kildishev, "Negative index of refraction in optical metamaterials," *Opt. Lett.* **30**, 3356–3358 (2005).
- E. Cubukcu, K. Aydin, E. Ozbay, S. Foteinopolou, and C. M. Soukoulis, "Subwavelength resolution in a two-dimensional-photonic-crystal based superlens," *Phys. Rev. Lett.* **91**, 207401 (2003).
- C. Y. Luo, S. G. Johnson, J. D. Joannopoulos, and J. B. Pendry, "Subwavelength imaging in photonics crystals," *Phys. Rev. B* **68**, 045115 (2003).
- C. Y. Luo, S. G. Johnson, J. D. Joannopoulos, and J. B. Pendry, "All-angle negative refraction without negative effective index," *Phys. Rev. B* **65**, 201104(R) (2002).
- C. Y. Luo, S. G. Johnson, J. D. Joannopoulos, and J. B. Pendry, "Negative refraction without negative index in metallic photonic crystals," *Opt. Express* **11**, 746–754 (2003).
- D. R. Smith, "How to build a superlens," *Science* **308**, 502–503 (2005).
- P. V. Parimi, W. T. T. Lu, P. Vodo, and S. Sridhar, "Photonic crystals—Imaging by flat lens using negative refraction," *Nature (London)* **426**, 404–404 (2003).
- Z. W. Liu, N. Fang, T.-J. Yen, and X. Zhang, "Rapid growth of evanescent wave by a silver superlens," *Appl. Phys. Lett.* **83**, 5184–5186 (2003).
- N. Fang, Z. W. Liu, T.-J. Yen, and X. Zhang, "Regenerating evanescent waves from a silver superlens," *Opt. Express* **11**, 682–687 (2003).
- A. Giannattasio, I. R. Hooper, and W. L. Barnes, "Transmission of light through thin silver film via surface plasmon-polaritons," *Opt. Express* **12**, 5881–5886 (2004).
- I. Gryczynski, J. Malicka, K. Nowaczyk, Z. Gryczynski, and J. R. Lakowicz, "Effects of sample thickness on the optical properties of surface plasmon-coupled emission," *J. Phys. Chem. B* **108**, 12073–12083 (2004).
- W. L. Barnes, W. A. Murray, J. Dintinger, E. Devaux, and T. W. Ebbesen, "Surface plasmon polaritons and their role in the enhanced transmission of light through periodic arrays of subwavelength holes in a metal film," *Phys. Rev. Lett.* **92**, 107401 (2004).
- Q. Cao and P. Lalanne, "Negative role of surface plasmons in the transmission of metallic gratings with very narrow slits," *Phys. Rev. Lett.* **88**, 057403 (2002).
- D. R. Smith, D. Schurig, M. Rosenbluth, S. Schultz, S. A. Ramakrishna, and J. B. Pendry, "Limitations on subdiffraction imaging with a negative refractive index slab," *Appl. Phys. Lett.* **82**, 1506–1508 (2003).